THESIS

HIGH-RATE GNSS SATELLITE CLOCK ESTIMATION: IMPLICATIONS FOR RADIO OCCULTATION BENDING ANGLE PRECISION

Submitted by

Yao-Chun Ko

Department of Electrical and Computer Engineering

For the Degree of Master of Science

Colorado State University

Fort Collins, Colorado

Fall 2024

Master's Committee:

Advisor: Haonan Chen
Co-Advisor: Jian Yao

Christine Chiu

ABSTRACT

HIGH-RATE GNSS SATELLITE CLOCK ESTIMATION: IMPLICATIONS FOR RADIO OCCULTATION BENDING ANGLE PRECISION

The Global Navigation Satellite System (GNSS) radio occultation (RO) technique plays a vital role in collecting data for meteorological and space weather prediction. It is exemplified by the COSMIC-2 low-Earth-orbit (LEO) satellite constellation, which collects the GNSS signals from an elevation angle of 90^{o} to below the horizon. Those GNSS observation data above 5^{o} elevation angle are used for the precise orbit determination of satellites, while those GNSS observation data below 5^{o} are used for the RO processing. A key part of the RO processing is to estimate the bending angle due to the atmospheric refraction, which requires an accurate information of the positions and clock offsets of both the transmitter (i.e., GNSS satellite) and the receiver (i.e., COSMIC-2 satellite). Previous research at University Corporation for Atmospheric Research (UCAR) [1] indicates a notable reduction in the intrinsic uncertainty of GLONASS radio occultation when employing higher-rate GNSS satellite clock products (e.g., from 30-second sampling interval to 2-second sampling interval). However, that work only analyzed one day of dataset. To analyze multiple days of dataset, I have developed a software program that can

automatically generate high-rate GNSS clock products by using a GNSS toolkit called GINAN [2]. This program is also important to the future UCAR's RO postprocessing and near-real-time processing. To be specific, it first downloads, merges, and decimates 1-second GNSS-receiver data from 50 worldwide ground stations, and then runs the GINAN software to generate clock products. I have validated the clock products generated by the program by comparing to International GNSS Service (IGS) analysis centers' clock products – the standard deviation of the time difference between our clock products and the clock products published by the Center for Orbit Determination in Europe is as small as ~ 0.1 nanoseconds. Using one week of 2-sec clock products generated by the program, I have run the standard RO processing and found that the bending-angle uncertainty of the GLONASS RO has been reduced by ~ 34%, as compared to if using the existing 30-sec clock products. Admittedly, there is no obvious improvement for the GPS RO because the GPS satellite clocks are stable at a short term of <= 30 seconds. By pushing down the noise of the RO technique, we can possibly observe the atmosphere at an unprecedented precision which could benefit the research of atmosphere modelling, the operation of weather monitoring and forecast, and even the study of space weather.

ACKNOWLEDGEMENTS

I would like to express my deep gratitude to my advisor, Dr. Haonan Chen, for his valuable guidance, patience, and unwavering support throughout my research in the Department of Electrical and Computer Engineering at Colorado State University. At the same time, I sincerely thank my co-supervisor, Dr. Jian Yao, for providing me with an excellent opportunity to do research and acquire satellite expertise at the University Corporation for Atmospheric Research (UCAR), and for supervising my master's research. I am grateful to the committee members, Dr. Haonan Chen, Dr. Jian Yao, and Dr. Christine Chiu. They gave me a lot of wonderful advice for enabling me to successfully complete my thesis and research. Their encouragement and strict standards motivate me to strive for excellence in my work and achieve the highest quality. I am also grateful to the staff of the Department of Electrical and Computer Engineering at Colorado State University for their administrative support and technical assistance that significantly aided my research.

I am grateful to the University Corporation for Atmospheric Research (UCAR), and in particular to Jan-Peter Weiss, Program Director of COSMIC, for his leadership and support of my research efforts. I would also like to thank Bill Schreiner for his advice and guidance on my research, Teresa VanHove for setting up the software environment needed for my research, and Dr. Yao, who has been not only my co-advisor but also a valuable Project Scientist II at UCAR to help

me complete the research. Their collective insights and encouragement contributed significantly to my research. I appreciate the staff of the University Corporation for Atmospheric Research (UCAR) and its COSMIC program for their assistance and for creating a conducive and friendly environment for my work.

The financial support provided by the University Corporation for Atmospheric Research (UCAR) has been integral to my studies and research. Their funding has enabled me to pursue my academic goals with greater focus and determination.

Finally, and most importantly, I would like to express my deepest gratitude to all my family members for their love, understanding, and constant encouragement throughout my educational journey. Their unwavering support has been my strength and motivation to achieve the completion of my thesis.

TABLE OF CONTENTS

ABSTRACT ii
ACKNOWLEDGEMENTS iv

Chapter 1 - Introduction 1
1.1 Global Navigation Satellite Systems (GNSS) 3
1.2 Radio Occultation (RO) on COSMIC-2 Satellites 6
1.3 GNSS Satellite Clock Estimate 10
1.4 Ginan Software 14

Chapter 2 - Methodology 17
2.1 High-Rate Clock Product Generated by Ginan Software 17
2.2 In-House Automation for Ginan Processing 21
2.3 Assessment of GNSS Bending Angle Measurements 23

Chapter 3 - Results 25
3.1 Ginan Clocks against CODE Final Clocks 25
3.2 Bending Angle versus Clock Estimation Rate..... 29

Chapter 4 - Conclusion and Future Works 34

REFERENCES 35

Chapter 1 – Introduction

The Global Navigation Satellite System (GNSS) Radio Occultation (RO) is an advanced technique in satellite remote sensing. It utilizes GNSS measurements obtained by satellites in low-Earth orbit (LEO) to accurately profile the Earth's neutral atmosphere and ionosphere. With a high vertical resolution, this technique provides a comprehensive global coverage of atmosphere observation and is essential to the monitoring and forecasting of both weather and space weather. The core part of the RO processing is to estimate the bending angle due to the atmospheric refraction. As illustrated in Figure 1, the bending angle is the direction change of the GNSS signal before and after transiting the Earth's atmosphere. The estimation of bending angle, which will be discussed in Section 1.3, requires accurate information of the positions and clock offsets of both the GNSS satellite and the LEO satellite. This thesis studies how to improve the bending angle estimation from the perspective of a higher sampling rate of GNSS satellite clocks.

This chapter provides a comprehensive introduction to the key concepts and technologies related to the research. In Section 1.1, I give an overview of Global Navigation Satellite Systems (GNSS), highlighting their significance and applications. Next, I'm going to introduce the estimation of GNSS satellite clock in Section 1.2. Then, I will explain the principles of Radio

Occultation (RO), a method used to probe the Earth's atmosphere in Section 1.3. Following this, the thesis examines techniques for estimating GNSS satellite clocks, which are crucial for accurate positioning and timing. Finally, I introduce the Ginan software together with its configuration, Kalman filtering process, and ambiguity estimation capabilities in Section 1.4. The subsequent chapters build on this foundation. Chapter 2 outlines the methodology, including the generation of high-rate clock products by Ginan software, automation of Ginan processing, and the assessment of GNSS bending angle measurements. Chapter 3 presents the results, comparing Ginan clocks with CODE final clocks, analyzing the relationship between bending angles and clock estimation rates, and providing detailed analyses of clocks and bending angles. The thesis concludes in Chapter 4 with a summary of findings and suggestions for future research directions.

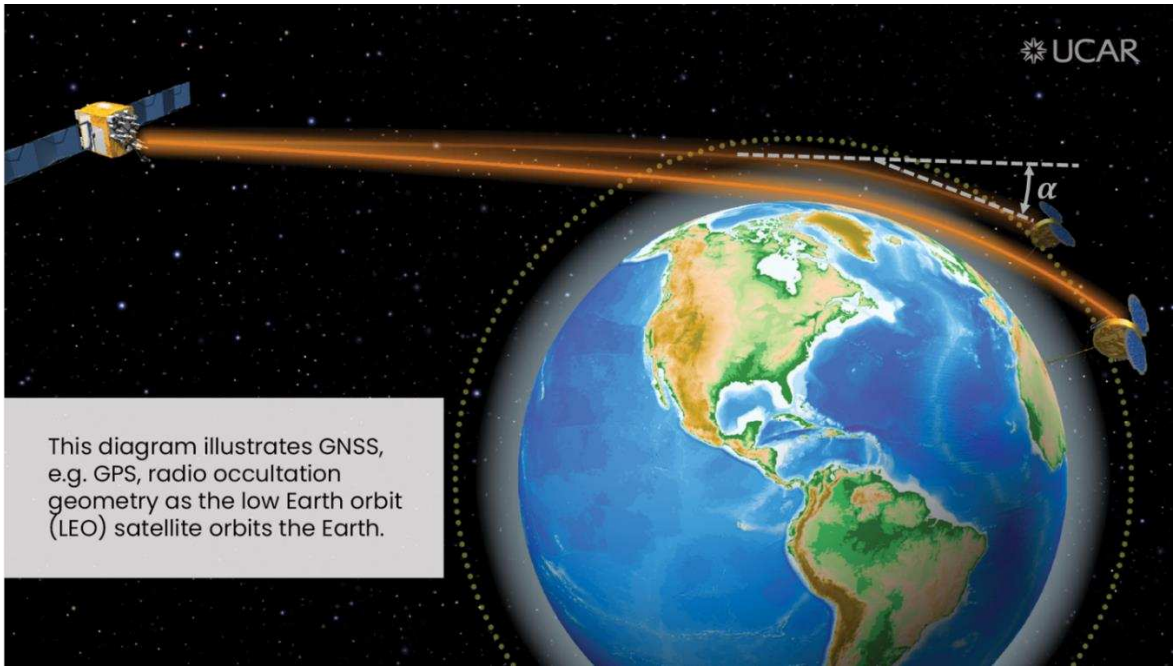

Figure 1: Illustration of the GNSS RO Geometry - the bending angle α is the direction change of GNSS signals as they pass through the Earth's atmosphere [3].

1.1 Global Navigation Satellite Systems (GNSS)

Global Navigation Satellite System (GNSS) includes several satellite constellations such as GPS, GLONASS, Galileo, and BeiDou, providing critical global positioning and timing services. These systems operate through a network of satellites that transmit signals with timestamps to receivers on the ground. For the GPS system, each satellite transmits at least two carrier waves (L1: 1575.42 MHz; and L2: 1227.60 MHz) with a code chipping rate of 1.023 MHz. A GNSS receiver can measure the time delay of signals from each GPS satellite, by doing correlation between the received satellite code and the receiver's local code at 1.023 MHz, which gives the "pseudo-range" to each satellite by multiplying the speed of light. Neglecting the additional delay due to the atmosphere or other physical effects, the pseudo-range measurement conducted by the receiver only depends on the distance between the satellite and the receiver, and the satellite and receiver clock offsets. Therefore, we can establish the following equation for each satellite-to-receiver link. This equation is also called "GNSS observation equation".

$$P_i^j = \left|\vec{x}^j - \vec{x}_i\right| - cT^j + cT_i \tag{1}$$

where $\left|\vec{x}^j - \vec{x}_i\right|$ is the distance between GNSS Satellite j and Receiver i, T^j is the satellite clock offset, and T_i is the receiver clock offset. The satellite position $\vec{x}^j$ and clock offset T^j are provided by decoding the GNSS satellite broadcast message. Therefore, we have four unknown variables in Equation (1) – receiver's position $\vec{x}_i$ and receiver's clock offset. If the

receiver can observe at least four satellites, then we can establish four equations as Equation (1) and thus can solve for the four unknowns. This is the basic principle of how to achieve positioning based on the GNSS system (see Figure 2 for the illustration).

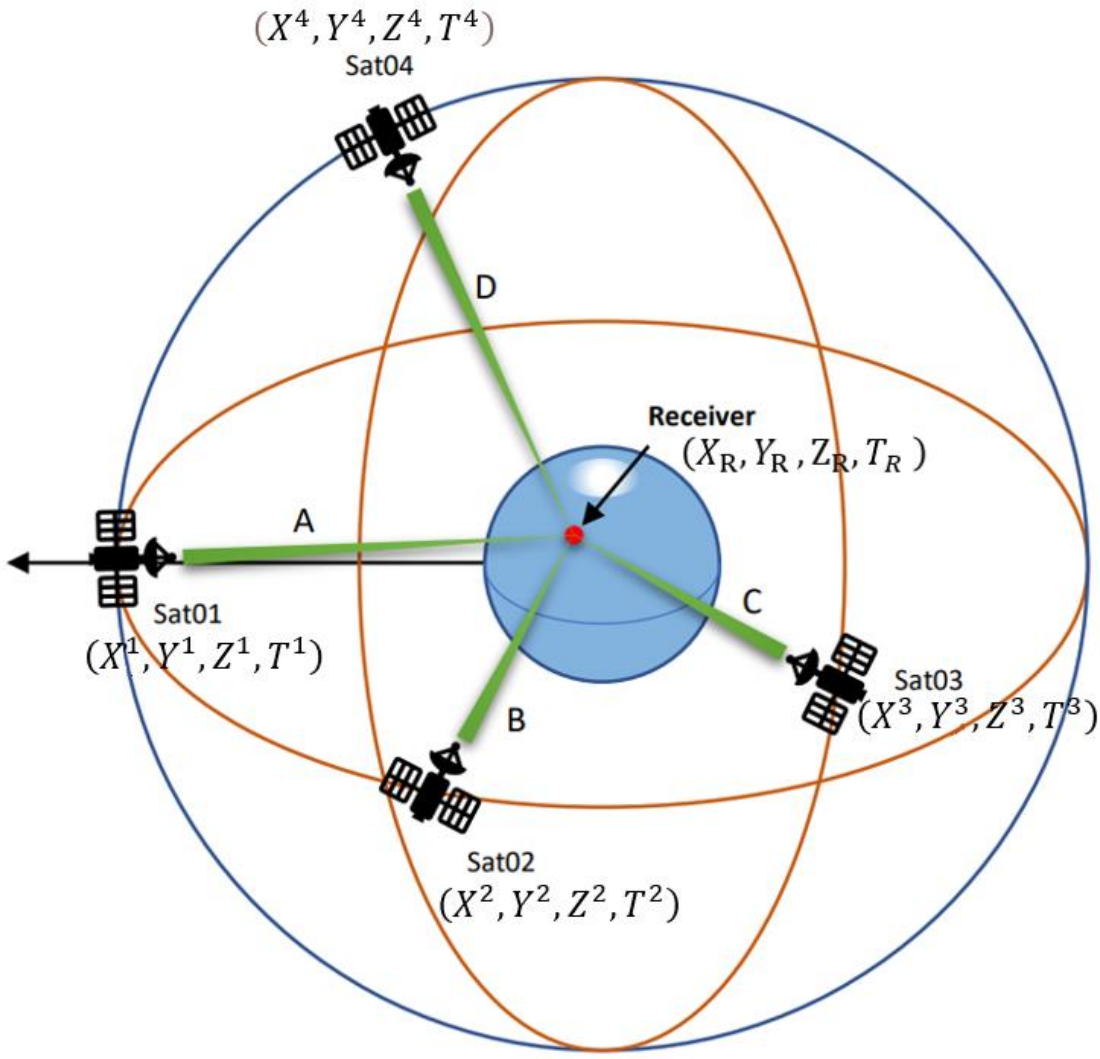

Figure 2: Illustration of the basic principle of GNSS Positioning [4]

Admittedly, many physical effects have impact on the pseudo-range [5]. For example, the troposphere and ionosphere lead to extra time delay in the signal path. A stricter version of

Equation (1) is expressed as follows,

$$P_i^j = \left|\vec{x}^j - \vec{x}_i\right| - cT^j + cT_i + \Delta_{ion} + \Delta_{tropo} + \Delta_{other\_P} + \varepsilon_P \quad (2)$$

where Δ_{ion} and Δ_{tropo} are the extra path delays due to the ionosphere and troposphere, respectively, Δ_{other} includes other physical effects such as satellite/receiver antenna delay, receiver's internal circuit delay, relativistic effect due to satellite's orbit eccentricity, etc. ε_P is the noise in the pseudo-range measurement.

To improve the precision of positioning and timing, the phase measurement that measures the phase difference between the received satellite carrier wave and the receiver's local carrier wave can be used. The precision is improved by orders of magnitude from the above code measurement, because the signal repetition rate changes from 1.023 MHz in code measurement to 1575.42 MHz or 1227.60 MHz in phase measurement [5]. The observation equation for the phase measurement is shown by Equation (3).

$$\Phi_i^j = \left|\vec{x}^j - \vec{x}_i\right| - cT^j + cT_i - \Delta_{ion} + \Delta_{tropo} + \Delta_{other\_\Phi} + \lambda N_i^j + \varepsilon_\Phi \quad (3)$$

Here, we have a minus sign in front of Δ_{ion} because the ionosphere results in phase advance rather than phase delay [5]. λ is the wavelength of the carrier wave and N_i^j is the phase ambiguity, which represents the total number of carrier-wave cycles between the satellite and receiver. Using many epochs of code measurements, we can have a good estimation of N_i^j and then keep it as a constant.

By assigning proper weights to Equations (2) and (3) (e.g., 1:100), we can have a precise and accurate estimation of receiver's position (typically several centimeters) and clock offset, given that we have good models of physical effects and long-enough receiver's measurement dataset (e.g., >= 2 hours).

1.2 GNSS Satellite Clock Estimate

In Section 1.1, we have discussed the basic principle of how to achieve the ground positioning, using known positions and clock offsets of GNSS satellites. The quality of GNSS satellite positions and clock offsets directly impacts the ground positioning performance as well as many other GNSS applications.

The broadcast message provides the satellite positions and clock offsets at an accuracy of a few meters. To improve accuracy and precision, the International GNSS Service (IGS) has established a ground network composed of hundreds of GNSS receivers that conduct both pseudo-range and phase measurements every 30 seconds. Therefore, we can establish millions of Equations (2) & (3). In such a huge equation set, we can solve for all unknown variables such as satellites' positions & clock offsets, receivers' positions & clock offsets, and even some troposphere & ionosphere parameters, after having a few minimum constraints on the coordinate system and timing system. The accuracy and precision of IGS-published satellite positions & clock

offsets is at the level of 2 centimeters or even better [6].

Nevertheless, IGS provides these high-quality satellite positions & clock products with some latencies. For example, the IGS rapid products have a latency of 17 hours [7]. To mitigate this issue, IGS has published ultrarapid products that have 24 hours of orbit & clock prediction. The predicted orbit typically has a good accuracy because satellite orbit is governed by gravitational forces together with other forces such as solar radiation pressure (SRP) force. These forces have been modeled very well. The clock prediction is challenging since the clock behavior is rather unpredictable. IGS real-time service (RTS) is mainly GPS-oriented and the quality of RTS products is out of the control of users.

At UCAR, we conduct the operational GNSS RO processing to support the weather and space weather monitoring & forecast. We generate our RO products in both near-real-time (< 30 min latency) and post-processing modes. The GNSS satellite orbit & clock products are core inputs of this processing. As mentioned earlier, the IGS ultrarapid orbit products are good enough for our near-real-time processing and the satellite orbit can be interpolated from 30 seconds to 1 second with little uncertainty thanks to the known forces on satellites. Also, several IGS analysis centers, such as GFZ, CODE, JPL, make their ultrarapid orbit products accessible to worldwide users, which further improves the robustness of our RO processing. For clocks, because of random clock behavior, the prediction portion of ultrarapid clock products is not enough to guarantee the high

quality of our RO products and thus we need to have our in-house estimation of satellite clocks rather than depending on the prediction of satellite clocks. We should mention that JPL has recently generated their near-real-time clock products covering the GPS constellation. They also plan to extend to other constellations. Nevertheless, from the operational perspective of a RO processing center like UCAR, it is still necessary to generate our in-house clock products to maintain a high level of independence and robustness. We currently use the Bernese GNSS software package to generate clock products at 30-second sampling interval with a latency of less than 10 min. We use several servers in Boulder, CO and Cheyenne, WY to do the same clock processing to improve the system robustness. [1] shows that higher-rate GNSS satellite clock products (e.g., 2 second per data point rather than 30 second per data point) can reduce the uncertainty of RO processing, especially for GLONASS RO since GLONASS satellite clocks are noisy at a short term. Therefore, we would like to generate 2-second clock products automatically to better fulfill our RO mission. In this section, we review the basic principle of GNSS satellite clock estimation.

A simple mathematical operation of Eq. (2-3) gives the following equations [8]. The left side of Eq. (4-5) is the time difference between Satellite *j* and Receiver *i*.

$$T^j - T_i = \frac{|\vec{x}^j - \vec{x}_i| - P_i^j + \Delta_{ion} + \Delta_{tropo} + \Delta_{other\_P} + \varepsilon_P}{c} \tag{4}$$

$$T^j - T_i = \frac{|\vec{x}^j - \vec{x}_i| - \Phi_i^j - \Delta_{ion} + \Delta_{tropo} + \Delta_{other\_\Phi} + \lambda N_i^j + \varepsilon_\Phi}{c} \tag{5}$$

Note that the ionosphere delay Δ_{ion} is a function of carrier wave frequencies. A dual-

frequency GNSS receiver conducts measurements at both L1 (1575.42 MHz) and L2 (1227.60 MHz). Therefore, we can estimate Δ_{ion} and then eliminate its impact. [5] provides details on how to form the ionosphere-free combination to get rid of the Δ_{ion} term. With the ionosphere-free combination of pseudo-range measurements and phase measurements (labelled as $P_i^j(ionfree)$ and $\Phi_i^j(ionfree)$, respectively), we can get Eq. (6-7),

$$T^j - T_i = \frac{|\vec{x}^j - \vec{x}_i| - P_i^j(ionfree) + \Delta_{tropo} + \Delta_{other\_P} + \varepsilon_P}{c} \tag{6}$$

$$T^j - T_i = \frac{|\vec{x}^j - \vec{x}_i| - \Phi_i^j(ionfree) + \Delta_{tropo} + \Delta_{other\_\Phi} + \lambda N_i^j + \varepsilon_\Phi}{c} \tag{7}$$

A clock from either the satellite system or the ground-receiver network needs to be chosen as the reference time. Its time offset is set to be zero at all epochs. Using Eq. (6-7), we can estimate the time offsets of the rest satellite and receiver clocks.

As mentioned in Section (1.1), Eq. (6) gives a coarse clock estimation because of large pseudorange-measurement noise ε_P, though its clock estimation is accurate because of no phase ambiguity term N_i^j involved. In contrast, Eq. (7) gives a fine clock estimation thank to the high precision of phase measurements, but the clock accuracy is limited due to phase ambiguity. The algorithms in GNSS software packages combine Eq. (6) & (7) appropriately so that we can achieve both high accuracy and precision of clock estimation.

A conventional GNSS receiver typically conducts pseudorange and phase measurements every 30 seconds, which enables the clock estimation every 30 seconds from Eq. (6-7). Nowadays,

many receivers have started to collect the measurement data at a higher sampling rate (e.g., 1 second per data point). A higher sampling rate allows the capture of subtle clock variations. Practically, due to the time consumption of data processing and limited computation resources, I implement 2-second clock estimation and study its impact on the RO processing at UCAR.

1.3 Radio Occultation (RO) on COSMIC-2 Satellites

Building upon the principles discussed in Section 1.2 on GNSS satellite clock estimation, where the receiver technology has enabled higher sampling rates for more frequent clock estimation, introduce radio occultation (RO) and explore how the high-rate clock estimation would impact RO in principle.

When GNSS radio signals pass through the atmosphere, they are bent or refracted toward the Earth's surface due to the vertical gradient of the refractive index. This bending causes a time delay, which can be measured by the phase shift of the radio signals, beyond the expected phase shift based on the relative position of the two satellites. The resulting refraction or ray bending angle can be computed from this additional phase shift. Note that the bending angle is exaggerated for illustrative purposes in Figure 1. It is typically about 1° near the Earth's surface and decreases exponentially with altitude. For a LEO satellite, sampling the radio signal from an altitude of around 100 km down to the surface takes about 1 to 2 minutes [9].

Figure 1 demonstrates how signals transmitted from GPS satellites are received by low Earth orbit (LEO) satellites. The bending and delay of these signals provide essential information for analyzing atmospheric conditions, such as atmospheric temperature, pressure, and humidity. The phase path of the signal L, which represents the actual refracted path, is calculated by integrating the refractive index n over the signal path ds between the GPS and LEO satellites as shown by Equation (1.8):

$$L = \int_{GPS}^{LEO} n \bullet ds \tag{1.8}$$

where L is the phase path length, n is the refractive index of the medium through which the signal travels [10]. The integral sums the product of the refractive index and the path element over the entire path from the GPS satellite to the LEO satellite. and This phase path deviates from the expected straight-line path. The difference between the measured phase path and this straight-line distance is termed the excess phase path ΔL as the Equation (1.9):

$$\Delta L = L - |\vec{x}_{LEO} - \vec{x}_{GPS}| \tag{1.9}$$

where ΔL is the excess phase path, and $|\vec{x}_{LEO} - \vec{x}_{GPS}|$ is the straight-line distance between the position of the LEO satellite (X_{LEO}) and GPS satellite (X_{GPS}) [10]. This excess phase path causes an excess Doppler shift that is distinct from the Doppler shift predicted purely by the relative velocities of the satellites. The excess Doppler shift is expressed as the time derivative of the excess phase path as the equation (1.10):

$$excess\ Doppler\ shift = \frac{d(\Delta L)}{dt} \tag{1.10}$$

where $\frac{d(\Delta L)}{dt}$ is the rate of change of the excess phase path with respect to time. This excess Doppler shift has a mathematical relation to the bending angle. Chapter 7 of [11] provides details on how to compute bending angle using the excess Doppler shift.

The accuracy of GNSS radio occultation bending angle retrievals is affected by various factors, such as thermal noise from the onboard GNSS receiver and antenna of the LEO satellite, as well as errors in the satellite clocks and orbits [12]. Residual errors persist in the bending angle after ionospheric corrections are applied to the L1 and L2 frequencies [13]. In addition, inaccuracies in the LEO satellite's attitude and the antenna phase center can further affect bending angle estimation. The actual signal path L in Eq. (1.8) is measured by the time delay from the GNSS satellite to the LEO satellite multiplied by the speed of light. To have an accurate time delay measurement, we need to know the time of GNSS satellite clock and the LEO satellite clock. A high-sampling rate clock estimation would improve the performance of the measurement of L, and thus affect the RO result.

This paper is based on the preliminary exploration of the influence of GNSS satellite clock sampling rate on bending angle accuracy using COSMIC-2 (Constellation Observing System for Meteorology, Ionosphere, and Climate-2) in [12] and [1]. COSMIC-2 is an advanced satellite mission dedicated to enhancing our understanding of Earth's atmosphere and ionosphere. This

mission, launched on June 25, 2019, represents a significant collaboration between the United States' National Oceanic and Atmospheric Administration (NOAA) and Taiwan's National Space Organization (NSPO). Comprising a constellation of six small satellites in low Earth orbit (LEO) at approximately 520 km altitude, COSMIC-2 leverages cutting-edge GNSS Radio Occultation (GNSS-RO) technology to provide critical data for weather forecasting, climate monitoring, and ionospheric research. The primary objective of COSMIC-2 is to improve global weather forecasting capabilities by measuring temperature, pressure, and humidity profiles of the atmosphere through 100 Hz sampling rate to capture GPS and GLONASS signals as they pass through various atmospheric layers. This GLONASS data, assimilated into numerical weather prediction models, significantly enhances the accuracy and reliability of weather forecasts, particularly in tropical regions where traditional observation methods are less effective. In Section 3.2. there are some results of RO which are computed by COSMIC-2 using 2-second clock products.

For the study of [12], it evaluates the impact of GPS and GLONASS clock interpolation on the retrieval of bending angles by RO. theoretically. Also, [1] analyzed one-day of real data and found that the intrinsic uncertainty of GLONASS radio occultation was reduced by using higher-rate GNSS satellite clock products. The improvement for GPS radio occultation is negligible due to the higher stability of GPS satellite clocks over short intervals. Based on these two studies, I

pick up 50 globally-distributed stations to estimate the 2-second clock for one week. Note that 50 stations are used in my study compared to 30 stations used in [1], which improves the robustness of clock processing. Then, I conduct the standard RO processing using one week of clock data and discover that the bending-angle uncertainty of the GLONASS RO was reduced by approximately 34% compared to using the existing 30-second clock products.

1.4 Ginan Software

Building on the basic concepts introduced in the previous sections, Section 1.4 delves into an integrated Global Navigation Satellite System (GNSS) software which is called Ginan. Ginan represents a complex application that utilizes the underlying theory discussed in Sections 1.1 to 1.2 to provide accurate and reliable GNSS data processing. This section will explore how Ginan improves high-frequency clock estimation by utilizing the precise satellite positioning and clock offset necessary for GNSS, and the detailed clock estimation technology necessary for high-precision applications, thereby improving the performance of RO (Section 1.3) for atmospheric observations.

Ginan is a comprehensive and powerful GNSS toolkit. It provides flexibility in handling file-based inputs for post-processing applications to achieve many data analysis needs. First, according to the inputs for clock generation, we need the following satellite measurements. For

example, the Solution Independent Exchange Format (SINEX) provides combined solutions for station coordinates and Earth orientation parameters, while Earth Rotation Parameters (ERP) track Earth's rotation and polar motion. Broadcast Ephemeris Data (BRD) contains the orbital parameters of GNSS satellites as broadcast to receivers, while Standard Product #3 (SP3) provides precise satellite orbit information. Differential Code Bias (BIA) is crucial for applying correction factors to address biases in satellite and receiver hardware, and the Receiver Independent Exchange Format (RNX) is the satellite observation data collected by the receivers.

The above introduces many processes and key input materials related to the operation of Ginan. Inside Ginan, it uses the Kalman filter to estimate parameters based on this information. The Kalman filter is an essential and efficient mathematical technique used for state estimation in dynamic systems. It integrates a mathematical model of the system with real-world measurements to make precise predictions about the system's state. By accounting for the noise and uncertainties in both the model and the observations through covariance matrices, the Kalman filter provides optimal estimates [14].

In the configuration for GNSS satellite clock estimation, the parameter "process noise" plays critical roles in the performance of the estimation process for satellite’s clock and its clock rate, managed by a Kalman filter. The " process noise " parameter, denotes the expected clock variability or uncertainty from the previous epoch to the current epoch in the process model itself,

capturing the inherent unpredictability of the system's dynamics. This parameter enables the Kalman filter to balance the trust between observed measurements and the model's predictions, ensuring accurate and reliable estimation of the satellite clock and clock rate, which are essential for high-precision GNSS data processing.

Also, accurate GNSS data processing challenged by carrier phase ambiguities (see Eq. (7)) —unknown wavelengths between the satellite and receiver. The Kalman filter addresses this need by providing forwardly iterative estimates of ambiguities, using both Eq. (6) and (7). Starting with an initial guess, the Kalman filter continuously updates its estimates using new pseudorange and phase measurements. By applying statistical methods, the filter minimizes estimation errors, dynamically adjusting to reduce uncertainty in the carrier phase ambiguities. This iterative process filters out noise and improves accuracy, making the Kalman filter indispensable for achieving precise GNSS-based clock estimation.

With the above backgrounds, we will discuss our methodology, results, and conclusions in the following chapters.

Chapter 2 – Methodology

In this section, a comprehensive and detailed overview of Ginan's process for efficiently producing high-rate clock products will be provided, including Ginan's operation, automated procedures, and evaluation and verification of bending angles. Chapter 2.1 focuses on Ginan's basic parameter adjustments that are critical to achieving clock accuracy, including the selection of satellite datasets provided to Ginan, adjustments of clock parameters, estimated epoch adjustments. Chapter 2.2 describes the operating mechanism that supports Ginan automated program execution. This subsection provides an in-depth introduction to the software architecture, data processing algorithms, and automated workflows that enable Ginan to process large amounts of GNSS data. Finally, Chapter 2.3 discusses the use of Ginan high-rate clock products to generate bending angles, and then performs a comparative analysis of clock products with different clock frequency, and at the same time will evaluate the quality of Ginan clocks in Section 3.1.

2.1 High-Rate Clock Product Generated by Ginan Software

In this study, I utilized the format of Yet Another Markup Language (YAML) configuration from the Ginan example, which focuses on post-processed network clock and bias estimation through GPS and GLONASS observations.

First, selecting good data quality of satellite measurements which was mentioned in Section 1.4 for Ginan's input use is an important step for this project. I obtain them from The Crustal Dynamics Data Information System (CDDIS) [15]. It is worth mentioning that one of the critical measurements is the observation data of the 50 ground receivers I selected since good quality and sufficient observation data are helpful in the estimation of satellite clocks. The list of our 50 receivers is as follows, ABMF, AREG, CEDU, CPVG, DAEJ, DARW, DAV1, DRAO, DUBO, FAA1, FLRS, HARB, HERS, HOB2, IQAL, JOG2, KERG, KIR0, KOKV, KOUR, LPAL, MAC1, MAJU, MAL2, MATE, MELI, MGUE, NICO, NKLG, NRC1, NTUS, PTVL, RGDG, SALU, SAMO, SAVO, SCOR, SCUB, SGOC, SOLO, STFU, STJO, TOW2, UFPR, ULAB, URUM, VOIM, YAR3, YELL, YKRO. I also choose a GNSS station, called Pivot Station in YAML, as the reference time for GINAN's output clock data since Ginan compare the satellite clocks to this reference. Here, I select "CEDU" as the Pivot Station. For other input information such as the satellite orbits, earth rotation parameter (ERP), I use the data provided by the Center for Orbit Determination in Europe (CODE), an IGS analysis center. For Ginan's estimated parameter configuration, I adjusted the clock estimation parameters called process noise I mentioned in Section 1.4 and set the time interval to 2 seconds (or 5 seconds, or 30 seconds) so that we can generate corresponding clock products.

Next, in Section 1.4, the Kalman file is used to solve for the phase ambiguity by averaging many epochs of satellite observation. Therefore, there is a convergence behavior at the very beginning of the data processing. The convergence behavior usually lasts 30 min – 1 hour. To avoid this convergence problem, I add the last 2 hours of the previous day's measurements. In this way, we no longer see any convergence behavior for the whole day of the current day. As an example, to generate the clock product for August 1st,2021, I process data from 22:00:00, July 31st, 2021, to 23:59:59, August 1st, 2021.

Finally, I would like to discuss the computation burden of the GINAN clock processing. Initially, without automation and good hardware, it would have taken more than one day to produce a full day of 2-sec clock data using my personal laptop. After analyzing all the sources of time consumption and optimizing the settings of the laptop, the clock generation still took a lot of time to estimate clock data. Therefore, I believe that the hardware of the computer is the biggest factor to impact the computation time. Then, I assembled a powerful computer to support the clock generation. The three key parts of a computer are CPU, memory, and SSD. The CPU I choose is Intel® Core™ i7 processor 14700K. Its specification of the computer has 20 cores and 28 threads, and the max turbo frequency is 5.6 GHz. Regarding the memory size, to be able to process a large amount of satellite data at the same time, the memory is chosen to be 32 gigabytes (GB) with the specification of DDR5-6000 PC5-48000, which is enough to handle the entire day's observation

data. Also, to have the fastest speed for data reading and writing, the computer is equipped Samsung - 980 PRO 2 terabytes (TB) solid-state drive (SSD) with PCIe Gen 4 x4 whose maximum read speed is 7000 megabytes per second and maximum write speed is 5100 megabytes per second. As for the operating system, I use Ubuntu 20.04 recommended by Ginan version 1.5. For the processing-speed test purpose, I use this computer to generate a 1-second clock for August 1st, 2021, and check the performance of the computer. The average core usage is ~99%, and its frequency is up to 4.8 GHz. That means, Ginan uses nearly all CPU resource to compute the clocks. The memory usage is 2 GB, and the SSD works in low speed to write the clocks in a clock file since every one second of clock data is computed approximately 1 second. For the 26 hours of one-second clock data (this avoids the convergence issue as mentioned earlier), it takes ~ 22 hours to get the one-day clock for August 1st, 2021. For the case of 26-hour period with 2-second intervals, Ginan estimates 46800 epochs of clock data and it takes ~ 12 hours to finish the clock processing. For generating one-day 5-second clock, it takes about 5 hours. We can see that generating high-rate clock data is time consuming and thus it is necessary to develop a program that conducts the clock processing automatically. In next section, I will show how to the automation works and what benefits will get from the automation.

2.2 In-House Automation for Ginan Processing

In the previous section, I emphasized the importance of hardware and automation because this project involves a lot of data processing. I have established an automation using Python for this sequential and systematic process to assist in the generation of clock products. This automated procedure eliminates the manual operation which was very time consuming for processing such big data. To be specific, in the past manual operation, it was necessary to set up GINAN's configuration and manually select ground stations, which required a lot of effort to make decisions. In contrast, the automated program saves time in generating clock products and also enables the processing of multiple-day data more efficiently. The analysis of multiple-day clock products and RO results is important to further confirm the single-day-analysis conclusion in [1].

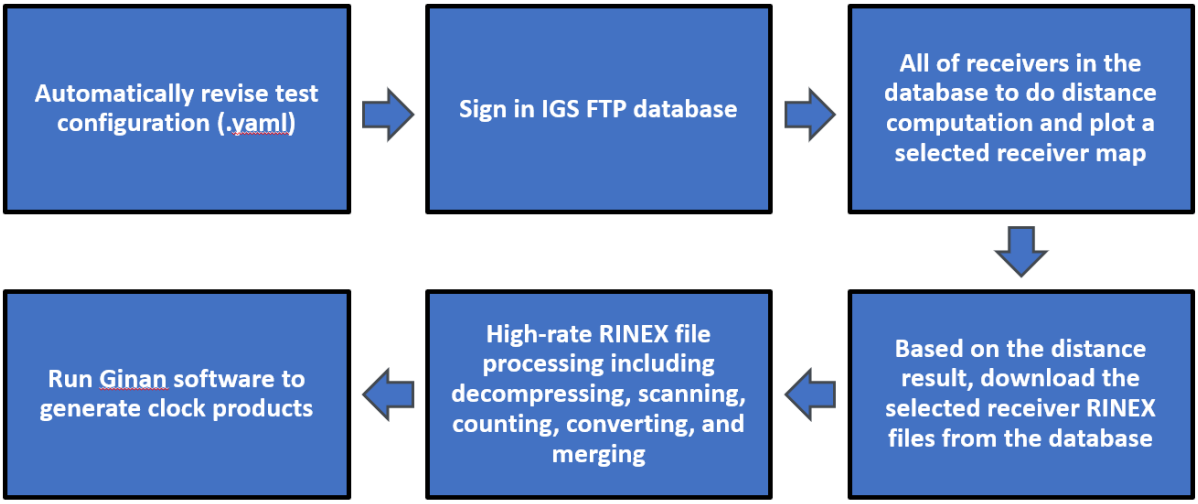

Figure 2: Workflow for Automated GNSS Data Processing with GINAN.

Here, I introduce my Ginan processing automation process by its flowchart (Figure 2). First,

a user needs to place an order that requires a clock date to be generated, then this program automatically reads the order and updates the configuration in the YAML file based on the given dates. Here, I use August 1st, 2021, as an example. The program automatically edits all date-specific input filenames for August 1, 2021, such as the "SNX" filename that provides the ground receivers' coordinates, the "ERP" filename for Earth rotation parameters, the "SP3" filename for satellite orbits, and the "RINEX" filenames which are the observation of satellites from each ground receiver, etc. In this way, the clock estimation can be ensured to proceed smoothly. After modifying the YAML file, the automation will go to the next stage -- signing in the IGS database, downloading all required input files and then processing the data. The IGS authorizes a user to log in the database via FTP. There is a large amount of GNSS data and products. Once automation gain access, it conducts a comprehensive search for the input files listed in the database and then downloads those files. Here I would like to mention the choice of ground receivers' observation, specifically. I have created an algorithm to calculate the distance among receivers recorded in SNX file, which is used to ensure that all receivers are (almost) evenly distributed on the Earth. That good distribution of receiver network enables a good visible and enough observation of each GNSS satellite. Next, the program handles all files downloaded at the user's computer. In particular, the receivers' high-rate observation data provided by the "RINEX" files need a series of operations to be ready for the GINAN run -- decompressing, scanning the content and counting relevant data

points for the data quality check, converting file formats, and merging all data to cover 26 hours. With this prepared data, the program finally runs the Ginan software by entering a fewcommands and generates the clock product. In summary, this automation program I've developed is designed to be both efficient and time saving. It can handle large volumes of GNSS data, which is essential for our research applications.

2.3 Assessment of GNSS Bending Angle Measurements

Now that we have explained how to generate clock data, we will next explain how to evaluate GNSS bending angle estimation using Ginan's clock products and analyze its performance. Several factors contribute to the noise of bending angle estimation. One of the primary sources is the small-scale residual from "ionosphere-free" combination, which arises even after first-order ionospheric corrections applied to L1 and L2 GNSS measurements. Additional sources include receiver thermal noise and unaccounted variations in the GNSS clocks.

For analysis, bending angles are compared with a climatological model [16] at tangent point altitudes between 60-80 km, a region where the atmospheric contribution to the signal is minimal [17]. This comparison yields a mean value and a standard deviation for all epochs within a segment (i.e., a RO event that typically lasts several seconds to several minutes). The mean value is typically close to zero, which reassures that the observed bending angles align with the

theoretical model. The National Center for Atmospheric Research (NCAR) climatological model, which is based on long-term averages and does not account for high-frequency errors such as transmitter clock noise or low earth orbit (LEO) receiver thermal noise, presents a smooth angle with minimal jitter from one epoch to the next. Conversely, observed bending angles includes errors from multiple sources, making them less stable epoch-wise.

Hence, the standard deviation of the observed bending angles from the climatological model, denoted as "STDV," [1] serves as an indicator of the uncertainty inherent in the radio occultation (RO) technique. The STDV is a measure of the variability in the bending angles, capturing the level of epoch-to-epoch jittering caused by higher rate RO errors and other sources of noise [1]. This metric, calculated in microradians, becomes a critical tool for quantifying the precision of bending angle measurements. These individual STDVs are then compiled on a per-receiver or per-transmitter basis, providing a comprehensive overview of estimation accuracy throughout the GNSS RO system. The mean value of all individual STDVs within one day is an even better statistical metric that is used to characterize the RO performance in this thesis.

Chapter 3 – Results

This chapter is structured into two key sections. Section 3.1 delves into a detailed comparison between Ginan clocks and the final clock products provided by the Center for Orbit Determination in Europe (CODE). This comparison aims to highlight the precision and reliability of Ginan's clocks by evaluating their performance against an established standard. Various statistical measures and plots will be used to illustrate the agreement (and small discrepancies) between these two sets of clock products. Section 3.2 investigates how the noise in the bending angle, which is a critical parameter in atmospheric modeling and signal propagation, is influenced by the high-rate clock products.

3.1 Ginan Clocks against CODE Final Clocks

For the clock generated by Ginan to be used for subsequent RO measurements, we must verify whether its clock quality and performance match the time products produced by the GNSS Analysis Center in IGS. This time, we collected the clocks on August 1st, 2021, to analyze and verify Ginan clock products. Also, the differences between GNSS clocks are being shown to remove clock reference since each analysis center chooses its own reference clock to generate their clocks. Thus, to eliminate the reference clock, we calculate the clock difference between G02 and

G01 of GPS and the clock difference of R02 and R01 of GLONASS, in the Ginan's clock product. Similarly, for CODE's clock product, we perform the same calculation to obtain the clock difference between G02 and G01 and the clock difference between R02 and R01. Now, we have the difference between the two clocks of the GPS and GLONASS satellite pairs, respectively.

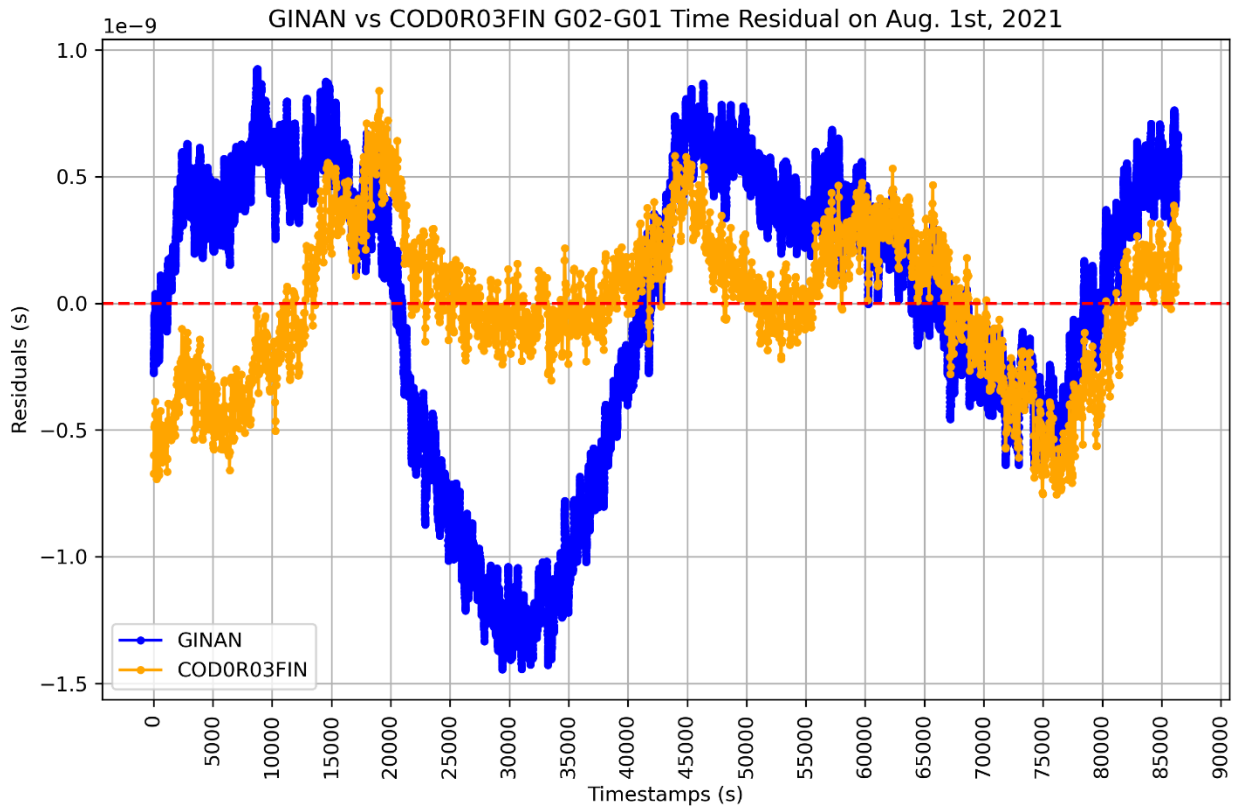

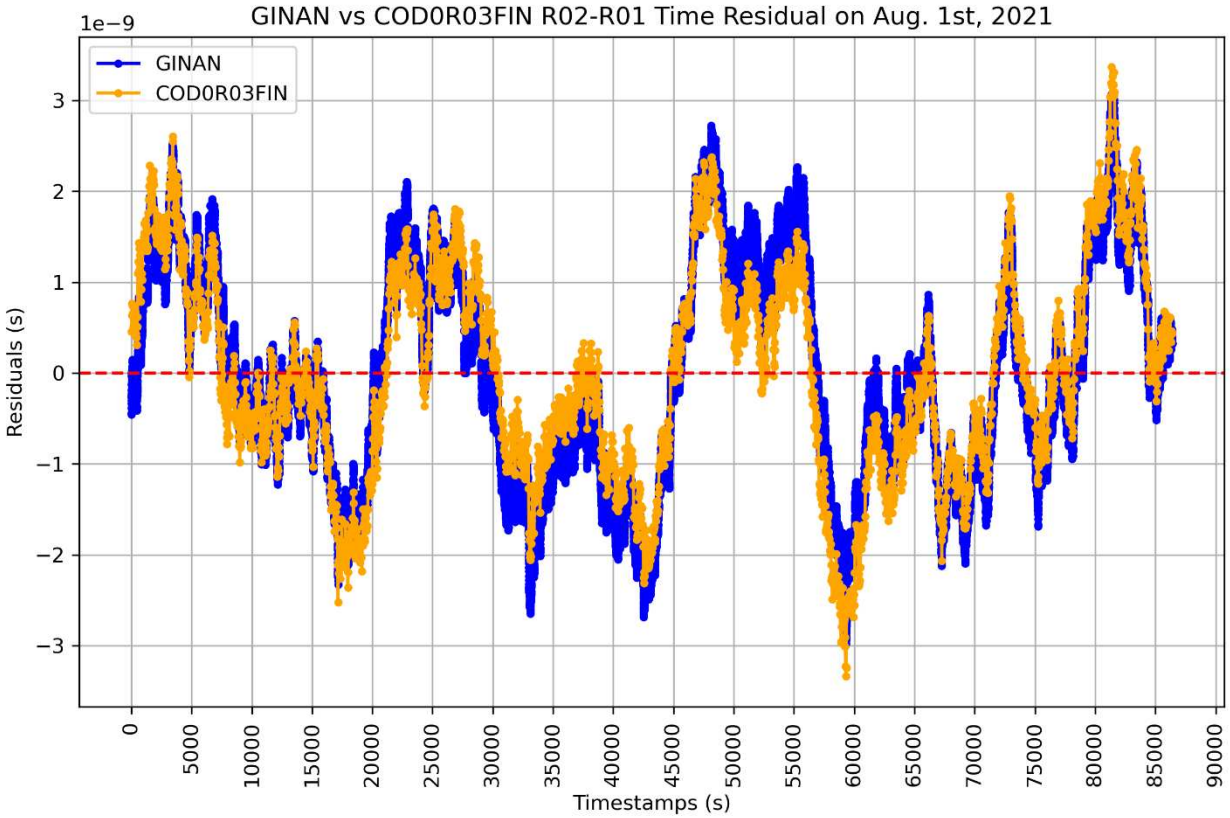

Figure 3: 30-Second Interval GNSS Clock Time Residuals of Ginan (in blue) and CODE (in orange) for GPS G02-G01 (Top) and GLONASS R02-R01(Bottom) on August 1st, 2021

For G02-G01 clock difference, there is a constant slope because each clock runs at a different rate. After removing this slope, we can see the residuals, which gives a better visualization of detailed clock behaviors (Figure 3). From Figure 3, the clock difference between these two GPS satellites is relatively consistent in both products, showing quite similar curve patterns. This implies that the GINAN-estimated "G02-G01" closely aligns with the CODE-estimate. It suggests a similar level of precision between the Ginan and CODE for these satellites. The bottom plot in Figure 3 shows the time residuals for the difference between GINAN's GLONASS satellites R02

and R01 as compared to the difference recorded by the CODE final product. The plot uses time and residual scales as the top plot. The time residuals for the R02-R01 difference from both Ginan and CODE display increased variability and larger deviations from zero. This suggests a more significant discrepancy and reduced stability in the time measurements between these two GLONASS satellites than what was observed for the GPS satellites in the earlier plot. Such inconsistency may lead to increased uncertainty in time-sensitive applications, including the calculation of bending angles for atmospheric profiling in radio occultation experiments. The highlighted instability for the GLONASS satellite time difference corroborates previous findings [1] regarding the relative instability of GLONASS clocks versus GPS clocks over short intervals of less than 30 seconds.

Table1. The STD Of GPS Clock Difference for GINAN's "X-G01" Minus CODE's "G0X-G01" on August 1st (X = No. of GPS, Unit: ns)

G02	G03	G04	G05	G06	G07	G08	G09	G10
0.59	0.24	0.21	0.66	0.47	0.32	0.33	0.31	0.49
G11	G12	G13	G14	G15	G16	G17	G18	G19
0.54	0.6	0.69	0.44	0.69	0.37	0.32	0.65	0.28
G20	G21	G22	G23	G24	G25	G26	G27	G28
0.6	1.8	0.18	0.64	0.62	0.49	0.5	0.47	0.41
G29	G30	G31	G32	Mean of GPS STD				
0.86	0.48	0.31	0.58	0.52				

Table2. The STD Of GLONASS Clock Difference for GINAN's "Y-R01" Minus CODE's "R0Y-R01" on August 1st (Y = No. of GLONASS, Unit: ns)

R02	R03	R04	R05	R07	R08	R09	R11
0.5	0.81	1.1	1.2	0.83	0.58	0.95	0.45
R12	R13	R14	R15	R16	R17	R18	R19
0.46	0.3	0.73	0.97	1.3	0.56	0.82	1
R20	R21	R22	R24	Mean of GLONASS STD			
1.2	0.91	0.56	0.41	0.78			

After comparing the GPS and GLONASS clocks produced by Ginan with CODE's final clock products mentioned above, their deviations are small than 1 nanosecond. Therefore, we confirm that our Ginan clock product is comparable to the CODE clock product and thus we can go to the next chapter 3.2 to further observe the impact of clock sampling rate on the bending angle. In the next section, I will analyze the changes in bending angles improved by using various Ginan clocks.

3.2 Bending Angle versus Clock Estimation Rate

In this section, I present two statistical tables, Table 3 and Table 4, which analyze the changes in the bending angle for each COSMIC-2 satellite under different clock rate scenarios.

Understanding the bending angle during specific events with different clock interval products is crucial. Table 3 focuses on a "setting event," representing the occurrence of radio occultation (RO) as the satellites move into the Earth's shadow. In contrast, Table 4 captures a "rising event," associated with RO when the satellites emerge from the Earth's shadow. These tables provide a detailed breakdown, including columns for the combined RO of the first COSMIC-2 satellite (S1), and separate columns for GPS-only RO (G) and GLONASS-only RO (R).

Table 3 and Table 4 provide a comprehensive comparison of the average standard deviation (STDV) values, measured in units of 1e-6 radians, for COSMIC-2 satellites during the setting and rising events on August 1st, 2021, across different clock rate scenarios: CODE-30s, Ginan-30s, Ginan-5s, and Ginan-2s. The Ginan-2s scenario, with a 2-second update interval, consistently achieves the lowest average STDV values, indicating superior clock accuracy across most satellites and systems. However, while the improvement for GPS-only data is minimal, the GLONASS-only data shows a significant reduction in STDV values, demonstrating a substantial enhancement in clock accuracy. This trend is further supported by the bending angle results, where the high-rate 2-second clock product from Ginan shows a noticeable reduction in bending angle values compared to the 30-second clock product, particularly for GLONASS-only radio occultation (RO) data and the overall average RO, confirming the effectiveness of the high-rate clock in achieving improved accuracy.

Table 3. Summary of **setting** "Avg of STDV" for All COSMIC-2 Satellites on August 1st in 2021 (Unit: 1e-6 radian)

Scenarios	S1	S1 (G)	S1 (R)	S2	S2 (G)	S2 (R)	S3	S3 (G)	S3 (R)	S4	S4 (G)	S4 (R)	S5	S5 (G)	S5 (R)	S6	S6 (G)	S6 (R)	Avg	Avg (G)	Avg (R)
CODE-30s	1.24	0.82	1.92	1.28	0.9	1.95	1.29	0.89	1.95	1.26	0.84	1.99	1.18	0.82	1.8	1.28	0.88	1.92	1.26	0.86	1.92
Ginan-30s	1.24	0.82	1.92	1.28	0.9	1.95	1.29	0.89	1.95	1.26	0.84	1.99	1.18	0.82	1.8	1.28	0.88	1.92	1.26	0.86	1.92
Ginan-5s	1.15	0.78	1.74	1.2	0.88	1.76	1.21	0.86	1.77	1.18	0.8	1.82	1.12	0.79	1.68	1.17	0.85	1.68	1.17	0.83	1.74
Ginan-2s	0.97	0.8	1.24	1.04	0.91	1.28	1.02	0.89	1.24	1.01	0.82	1.35	0.97	0.83	1.21	0.99	0.84	1.24	1	0.85	1.26

Table 4. Summary of **rising** "Avg of STDV" for All COSMIC-2 Satellites on August 1st in 2021 (Unit: 1e-6 radian)

Scenarios	S1	S1 (G)	S1 (R)	S2	S2 (G)	S2 (R)	S3	S3 (G)	S3 (R)	S4	S4 (G)	S4 (R)	S5	S5 (G)	S5 (R)	S6	S6 (G)	S6 (R)	Avg	Avg (G)	Avg (R)
CODE-30s	1.17	0.87	1.69	1.21	0.85	1.81	1.36	0.94	2.02	1.38	0.98	2.1	1.14	0.81	1.69	1.36	0.99	1.95	1.27	0.91	1.88
Ginan-30s	1.17	0.87	1.69	1.2	0.85	1.81	1.36	0.94	2.02	1.38	0.97	2.1	1.14	0.81	1.69	1.36	0.99	1.95	1.27	0.91	1.88
Ginan-5s	1.09	0.83	1.54	1.12	0.83	1.61	1.25	0.91	1.8	1.3	0.94	1.91	1.06	0.77	1.54	1.28	0.96	1.8	1.18	0.87	1.7
Ginan-2s	0.97	0.85	1.17	1	0.85	1.24	1.07	0.94	1.28	1.12	0.96	1.39	0.94	0.79	1.18	1.1	0.98	1.31	1.03	0.9	1.26

Moreover, to verify the improvement in bending angle accuracy, a 7-day Ginan clock was generated and analyzed over the period from August 1, 2021, to August 7, 2021. The results, presented in Tables 5 and 6, demonstrate the effectiveness of different scenarios in reducing the bending angle noise for COSMIC-2 satellites. The average standard deviation (STDV) of the bending angle was measured in units of 1e-6 radians.

Table 5 displays the settings for the "Avg of STDV" for all COSMIC-2 satellites under various scenarios. The baseline setup, CODE30s, showed an average STDV of 1.81 for GLONASS. The scenario Ginan-30s produced a similar result with an average STDV of 1.81. However, the Ginan-5s scenario demonstrated a noticeable improvement, with an average STDV of 1.65,

representing a decrease of approximately 8.8%. The most significant improvement was observed in the Ginan -2s scenario, which achieved an average STDV of 1.19, corresponding to a substantial reduction of about 34%.

Table 5. The average of setting “Avg of STDV” for All COSMIC-2 Satellites (Unit: 1e-6 radian)

Scenarios	Avg	Avg (G)	Avg (R)
CODE-30s	1.18	0.81	1.81
Ginan-30s	1.18	0.81	1.81
Ginan-5s	1.1	0.78	1.65
Ginan-2s	0.94	0.8	1.19

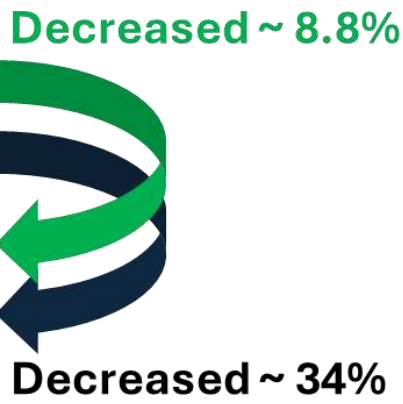

Similarly, Table 6 presents the rising "Avg of STDV" for all COSMIC-2 satellites. The baseline setup, CODE30s, had an average STDV of 1.87, while the Ginan-30s scenario maintained the same level of 1.87. The Ginan-5s scenario showed a reduced average STDV of 1.69, marking a decrease of approximately 9.6%. The Ginan-2s scenario once again achieved the greatest reduction, with an average STDV of 1.23, indicating a decrease of approximately 34%. Therefore, it is obvious that the higher rate clock helps to significantly reduce the uncertainty of bending angle estimation and thus improve the RO performance.

Table 6. The average of setting “Avg of STDV” for All COSMIC-2 Satellites (Unit: 1e-6 radian)

Scenarios	Avg	Avg (G)	Avg (R)
CODE-30s	1.26	0.88	1.87
Ginan-30s	1.25	0.88	1.87
Ginan-5s	1.17	0.85	1.69
Ginan-2s	1.01	0.88	1.23

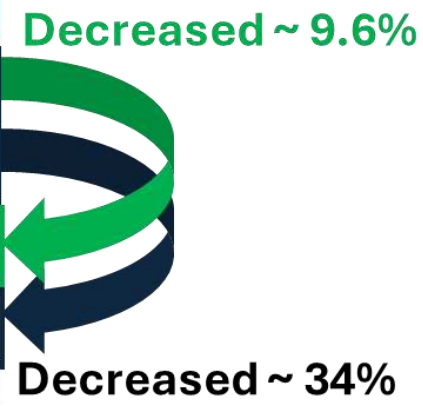

Chapter 4 – Conclusion and Future Works

The study concluded that estimating GNSS satellite clocks at higher rates, especially with intervals shorter than 30 seconds, can significantly improve the performance of GLONASS radio occultation (RO). GLONASS satellite clocks are known to be noisier and less predictable on timescales of 30 seconds or less compared to GPS satellite clocks. Therefore, the bending-angle noise reduction observed with higher rate clock estimates aligns with expectations. A significant improvement highlighted in this study is the use of Ginan's 2-second GNSS clocks which represents a GLONASS-RO improvement of approximately 34% compared to conventional 30-second clocks. The automated procedures customized for Ginan achieved the expected efficiency and greatly reduced manual operation time. I also finished using Ginan to produce a complete clock product from August 1, 2021, to August 7, 2021. Looking ahead, we have set several goals for our future work. We plan to explore the latest version of Ginan – Ginan 3.0, which may improve the reliability/robustness of Ginan operation. We also plan to implement this automation on UCAR servers for daily clock processing. Last, with an improved RO sensitivity, we would like to see if we can monitor the weather and space weather at a better accuracy.

REFERENCES

[1] Jian Yao, Jan-Peter Weiss, and Teresa VanHove, “Impacts of high rate GNSS satellite clock estimation on radio occultation bending angle retrievals: preliminary report,” Proceedings of the 2023 Institute of Navigation International Technical Meeting (ITM), pp. 995 – 1001, 2023.

[2] Rupert Brown, “GINAN project overview,” 2022.

[3] GNSS Radio Occultation, https://www.cosmic.ucar.edu/what-we-do/gnss-radio-occultation

[4] Rupert Brown, GINAN (Analysis Centre Software) Project Overview, September 2022, https://geoscienceaustralia.github.io/ginan/resources/GinanProjectOverview202209v01.pdf

[5] Pratap Misra, Per Enge, “Global Positioning System: Signals, Measurements and Performance, Revised Second Edition,” 2011.

[6] Jan Kouba, “A GUIDE TO USING INTERNATIONAL GNSS SERVICE (IGS) PRODUCTS,” 2015.

[7] The Products of International GNSS Service, https://igs.org/products/.

[8] Jian Yao, Sungpil Yoon, Bryan Stressler, Steve Hilla, and Mark Schenewerk, “GPS satellite clock estimation using global atomic clock network,” GPS Solutions, vol. 25, pp. 1-10, 2021.

[9] Hans Gleisner, Mark A. Ringer, Sean B. Healy, “Monitoring global climate change using GNSS radio occultation”, 2022.

[10] Stig Syndergaard, “Introduction to GPS Radio Occultation”, 2005.

[11] W. G. Melbourne, E. S. Davis, C. B. Duncan, G. A. Hajj, K. R. Hardy, E. R. Kursinski, T. K. Meehan, L. E. Young, T. P. Yunck, “The Application of Spaceborne GPS to Atmospheric Limb Sounding and Global Change Monitoring”, 1994.

[12] Jan P. Weiss, Sergey Sokolovskiy, Bill Schreiner, and Yoke Yoon, “GNSS clock interpolation impacts on radio occultation bending angle retrieval,” IGS Workshop, 2017.

[13] Keshav R. Tripathi, R. K. Choudhary, “Quantification of Errors in the Planetary Atmospheric Profiles Derived from Radio Occultation Measurements”, 2022.

[14] McClusky, Simon, Hammond, Aaron, Maj, Ronald, Allgeyer, Sébastien, Harima, Ken, Yeo, Mark, Du, Eugene, Riddell, Anna, "Precise Point Positioning with Ginan: Geoscience Australia’s Open-Source GNSS Analysis Centre Software," Proceedings of the ION 2024 Pacific PNT Meeting, Honolulu, Hawaii, April 2024, pp. 248-280. https://doi.org/10.33012/2024.19598

[15] About the CDDIS GNSS data and products Archive, https://cddis.nasa.gov/Data_and_Derived_Products/GNSS/GNSS_data_and_product_archive.html

[16] William Randel, Petra Udelhofen, Eric Fleming, et al, “The SPARC intercomparison of middle-atmosphere climatologies,” Journal of Climate, vol. 17, pp. 986-1003, 2004.

[17] Andrea K. Steiner, Florian Ladstädter, Chi O. Ao, et al, “Consistency and structural

uncertainty of multi-mission GPS radio occultation records," Atmos. Meas. Tech., vol. 13, pp. 2547-2575, 2020.